Research Square

Preprints are preliminary reports that have not undergone peer review.
They should not be considered conclusive, used to inform clinical practice,
or referenced by the media as validated information.

Hydrogel Microparticles Preserve Cell Secretome and Extracellular Vesicle Bioactivity for Improved Cell-Based Therapy Deployment

Li Ching Wong
Food, Chemical and Biotechnology Cluster, Singapore Institute of Technology, Singapore
Craig Jun Kit Wong
National University of Singapore
Kwan Yu Wu
National University of Singapore
Serene Ming En Chong
Food, Chemical and Biotechnology Cluster, Singapore Institute of Technology, Singapore
Yee Kit Tai
alextai@nus.edu.sg

National University of Singapore
Rufaihah Abdul Jalil
School of Applied Science, Temasek Polytechnic, Singapore
Arif Z. Nelson
arif.nelson@singaporetech.edu.sg

Food, Chemical and Biotechnology Cluster, Singapore Institute of Technology, Singapore
Alfredo Franco-Obregón
afo@nus.edu.sg

National University of Singapore

Research Article

Keywords: conditioned media, pulsed electromagnetic fields, stem cells, microgel, regenerative medicine

Posted Date: March 4th, 2026

DOI: https://doi.org/10.21203/rs.3.rs-9015333/v1

License: This work is licensed under a Creative Commons Attribution 4.0 International License.
Read Full License

Additional Declarations: The authors declare potential competing interests as follows: Author AF-O reports being a contributor to QuantumTx Pte. Ltd., which elaborates electromagnetic field devices for human use. Author AF-O is an inventor on patent WO 2019/17863 A1, System and Method for Applying Pulsed Electromagnetic Fields. Authors AF-O, CJKW, YKT, and RAJ are inventors on patent WO 2024/005714 A1, Directionally-specific Magnetic Modulation of the Cell Secretome for Medical and Commercial Applications. All Authors are inventors on patent WO/2025/212041, Collapsible cell-encapsulating scaffolds to enhance magnetically-induced secretome stabilisation and potency. There are no other known competing financial interests or personal relationships that could have appeared to influence the work reported in this paper.

Hydrogel Microparticles Preserve Cell Secretome and Extracellular Vesicle Bioactivity for Improved Cell-Based Therapy Deployment

Li Ching Wong[a #], *Craig Jun Kit Wong*[b,c,d #], *Kwan Yu Wu*[b,c,d], *Serene Ming En Chong*[a], *Yee Kit Tai*[b,c,d,e]*, *Rufaihah Abdul Jalil*[b,f,g], *Arif Z. Nelson*[a]*, *and Alfredo Franco-Obregón*[b,c,d,e,h]*

[a]Food, Chemical and Biotechnology Cluster, Singapore Institute of Technology, Singapore
[b]Department of Surgery, Yong Loo Lin School of Medicine, National University of Singapore, Singapore;
[c]Institute of Health Technology and Innovation (iHealthtech), National University of Singapore, Singapore;
[d]Biolonic Currents Electromagnetic Pulsing Systems Laboratory (BICEPS), National University of Singapore, Singapore
[e]NUS Centre for Cancer Research, Yong Loo Lin School of Medicine, National University of Singapore, Singapore
[f]Healthy Longevity Translational Research Programme, Yong Loo Lin School of Medicine, National University of Singapore, Singapore;
[g]School of Applied Science, Temasek Polytechnic, Singapore
[h]Competence Center for Applied Biotechnology and Molecular Medicine, University of Zürich, Switzerland
[#]Li Ching Wong and Craig Jun Kit Wong contributed equally to this work.

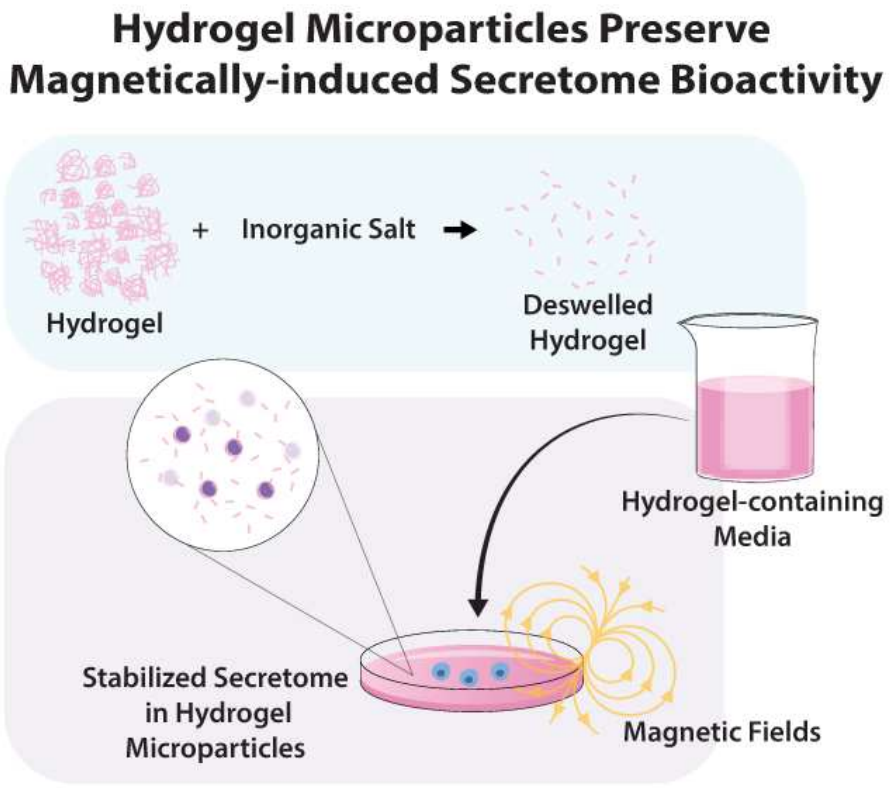
***Corresponding author**
e-mail: afo@nus.edu.sg (Alfredo Franco-Obregón); arif.nelson@singaporetech.edu.sg (Arif Z. Nelson); alextai@nus.edu.sg (Tai Yee Kit)
Postal address: Institute for Health Innovation and Technology, National University of Singapore, MD6, 14 Medical Drive, #14-01, Singapore 117599 (Alfredo Franco-Obregón and Tai Yee Kit); Singapore Institute of Technology, SIT Kwek Leng Beng University Tower (E1), 1 Punggol Coast Road, Singapore 828608 (Arif Z. Nelson)
Telephone: +65 66016143 (Alfredo Franco-Obregón and Tai Yee Kit); +65 6592 4613 (Arif Z. Nelson)

Keywords: conditioned media, pulsed electromagnetic fields, stem cells, microgel, regenerative medicine

Abstract

Secretomes derived from diverse progenitor cell classes are commonly employed in regenerative medicine applications to promote cell expansion and tissue differentiation. However, the bioactivity of secretome components, including soluble proteins and extracellular vesicles, is hindered by their low stability in basal cell culture media. Hydrogels are a promising strategy for improving secretome viability by providing a structurally supportive, biomimetic environment. This work examined the effects of poly(acrylic acid)-based hydrogel microparticles in the context of a previously characterised magnetic secretome-induction paradigm. We investigated the impact of a hydrogel microenvironment on the release and collection of secretome, during and after media conditioning. Various inorganic salt species were used to control microgel particle swelling and enable liquid phase collection. Calcium chloride was more effective than sodium or magnesium chlorides in facilitating secretome recovery with reference to promoting in vitro myogenesis at the cellular and protein levels. Notably, the secretome released from magnetically-induced myoblast cultures in microgel-derived conditioning media was as supportive of cell growth as foetal bovine serum (FBS), whereas the secretomes harvested from unstimulated cells in hydrogels or from stimulated cells in the absence of hydrogels were less effective. Microgel-derived conditioned media also enhanced the stability of isolated extracellular vesicles, better preserving their efficacy during storage at room temperature, 4° C and -20° C. These results indicate that these microgels protected the secretome from degradation. Media incorporating microgels represent an innovative approach with which to preserve the potency of cell secretomes collected following various induction protocols for improved commercial and clinical exploitation.

Graphical Abstract



1. Introduction

The cell secretome is comprised of a diverse collection of proteins and bioactive factors of broad trophic and metabolic implications. A growing body of research has been focusing on the therapeutic uses of the cell secretome, in particular of the vesicular component, for a wide range of biomedical applications including wound healing, immune modulation, and tissue engineering [1–3]. Despite these promising regenerative attributes a major barrier to the effective translation of cell secretomes is achieving viable yields sufficient to support cell growth and differentiation [4,5]. Two critical issues remain to be addressed in order to overcome this shortcoming: i) the development of efficient methods of inducing secretome release with a minimum of cellular stress and; ii) devising safe technologies and protocols for maintaining the potency of secretome components until their point of application.

Diverse methodologies have been devised to induce the release of the cell secretome. These methods range from the use of chemical agents, such as ionophores, to physical stimuli like

electrical or laser pulses, and even environmental triggers such as hypoxia [6–10]. Emerging evidence suggests that harsher induction methods, while potentially producing greater yields of secretome, may compromise its bioactivity or even impart undesired effects [11]. In this regard, Pulsed Electromagnetic Fields (PEMF) may offer a gentler and non-invasive alternative. Brief exposure to PEMFs has been previously shown to enhance the myogenic potential of conditioned media (CM) generated from myoblasts in suspension and thus amenable to industrial bioreactor paradigms [12]. Specifically, a single 10-minute exposure to low-amplitude (1.5 mT) and low-frequency (15 Hz) PEMFs was shown to activate calcium entry via the transient receptor potential canonical 1 (TRPC1) channel that, in turn, stimulates PGC-1α-mediated transcriptional cascades [13,14]. Of noted relevance to the present study, the PGC-1α transcriptional cascade governs the cellular secretome response [15,16]. Accordingly, PEMF exposure of this form stimulates the production and release of muscle-derived secretome factors, including extracellular vesicle (EV) species [12,17]. The present study employed this previously characterized PEMF methodology of inducing secretome release [12,14,17,18]. Due to space considerations, a comparison of alternative forms of secretome induction is outside the scope of the present work.

Once released into the bathing media, maintaining the potency of the various secretome components, particularly EVs, is a major challenge. This is especially critical for applications requiring long-term storage and transportation [12,19]. Several preservation strategies have been developed to sustain the stability and bioactivity of secretome components, including low-temperature storage, incorporation of protective agents, and lyophilization [19–21]. In particular, hydrogels have emerged as a versatile approach of enhancing secretome stability by minimising aggregation and providing a biomimetic environment that supports cell growth in 3D cell culture [22–24]. Existing studies indicate that hydrogel-based 3D cell cultures enhance EV secretion relative to conventional two-dimensional culture conditions because they more closely mimic the *in vivo* microenvironment [25,26]. Additionally, the tuneable mechanical properties of hydrogels enable the controlled modulation of critical cellular culture conditions, thereby enhancing the secretory profiles of embedded cells.

Carbopol® (CP), or Carbomer, is the brand name of a family of hydrophilic partially crosslinked poly(acrylic acid) polymeric microparticles that swell in aqueous media in a manner that is sensitive to pH and ionic strength [27]. CP is FDA approved and listed in their Inactive Ingredient

Guide (IIG) for oral, topical, and ophthalmic pharmaceutical deployment. CP is widely utilized as a rheology modifier to improve the consistency and viscosity of pharmaceutical and cosmetic products, effectively suspending dispersed components in an aqueous media [28–30]. Carbopol's safety profile has led to its use as an adjuvant and stabilizer in live-attenuated vaccines for animals [31,32]. At sufficiently high concentrations in solution, CP microgels pack against one another, forming a jammed suspension and a yield-stress fluid [33,34]. Moreover, the biocompatibility and complex rheological behaviour of CP microgel suspensions (hereafter referred to as CPG) satisfy essential requirements for cells in culture, making them applicable as a bioink in 3D cell culture [35–37] or as supporting baths for bioprinting [37]. Beyond supporting cells, the tuneable rheology offered by CP facilitates the creation of 3D culture environments that better approximate *in vivo* environments, allowing for the free diffusion of nutrients and small molecules within complex fluids to supply trophic and metabolic needs of the cell [35,37]. Given its documented cytobiocompatibility and hydrogel-forming capabilities, CP can provide a supportive environment for cell culture as well as may enhance the stability of cell-secreted proteins for a wide range of clinical or commercial applications.

This study investigates the utilization of CP hydrogel microparticles to preserve secretome potency by leveraging established PEMF protocols for gently inducing secretome release [12]. We explored the potential of different strategies of delivering CP support to improve the stability and bioactivity of different PEMF-induced cell secretion components [12,14,17,18]. We identify a formulation which was best at providing a favorable environment for donor cell health and secretome release, as well as which proved the easiest and most convenient to deploy in commercial settings and with minimized exogenous contaminants. A workflow is presented for streamlining the recovery, bioavailability, and bioactivity of CM or EVs for their efficient provision to recipient cell cultures for enhanced regenerative potential.

2. Experimental materials and methods

2.1 Preparation of Carbopol® microgel (CPG) media formulations

Suspensions of CPG were prepared by mixing Carbopol® 974P NF (CP 974) (Lubrizol Corporation, Wickliffe, Ohio, United States) in basal media High glucose Dulbecco's Modified

Eagle Medium (DMEM; Cytiva SH30243.01; Cytiva, Marlborough, United States) at varying concentrations. After 1 h of stirring, the pH of the suspensions was adjusted to 7.4 by adding 1 M aqueous sodium hydroxide solution prepared from sodium hydroxide pellets (Sigma-Aldrich, St. Louis, Missouri, United States) under continuous stirring, resulting in a viscous suspension.

2.2 Characterization studies

2.2.1 Rheological characterization

All samples were degassed by using a vacuum chamber before rheological experiments. All rheological measurements were performed using a Discovery Hybrid Rheometer HR-30 (TA Instruments, New Castle, DE, USA) equipped with a Peltier temperature controller set to 37˚C to simulate cell culture conditions. Steady shear flow measurements were conducted using a concentric cylinder fixture (546011.941 HA Aluminum Conical DIN Rotor) with a 14 mm radius and 42 mm height. A range of shear rates was applied from 10 to 10^{-2} s^{-1} and the steady shear stress was recorded and fit to a Herschel-Bulkley (HB) model (Equation 1) using Origin 2024b.

$$\sigma = {\sigma_Y}^{HB} + K\dot{\gamma}^n \qquad \textbf{Equation 1}$$

where σ is shear stress, ${\sigma_Y}^{HB}$ is yield stress, K is consistency index, $\dot{\gamma}$ is shear rate and n is flow index.

2.2.2 Microscopy

The samples were observed using Axiovert 5 Inverted Microscope with Phase Contrast coupled to an Axiocam 208 color digital camera (Carl Zeiss, Germany). The images were saved using Zeiss Labscope 4.0 software. The sizes of CPG aggregates were obtained by using a MATLAB function [38].

2.2.3 Size determination and zeta potential measurement

Particle size distribution and zeta potential were analyzed using a Zetasizer Nano ZS (Malvern Panalytical, Malvern, UK). Particle size distribution was determined via Dynamic Light Scattering (DLS) using a disposable cuvette. Zeta potential was measured using disposable folded-capillary zeta cells (DTS1070; Malvern Panalytical, Malvern, UK) according to a modified method [39]. To prevent electrode degradation, measurements were conducted using a diffusion barrier of 1 mM NaCl at 25 °C to separate the sample from the electrodes. The zeta cell was equilibrated for 120 s prior to measurement, and a 120 s delay was used between successive runs. All measured electrophoretic mobilities were converted into zeta potential using Smoluchowski's equation, and the reported values represent the mean of five independent measurements, each comprising 20 individual scans.

2.2.4 Recovery of media from CPG formulations

To assess the efficiency of media recovery, the CPG media formulations were centrifuged at 6000 ×g for 15 min. The resulting CPS was then recovered via pipetting. Recovery efficiency was quantified as the volume of CPS collected relative to the total volume and expressed as a percentage.

To further enhance the recovery of cell-conditioned CPS (CM from CPS containing cell secretions), the CPG was deswelled with salts prior to centrifugation. This was achieved by adding $MgCl_2$, $CaCl_2$, and NaCl (Sigma-Aldrich, St. Louis, Missouri, United States) to predetermined concentrations. These salt concentrations were chosen to maximize media recovery while ensuring appropriate conditions for cell culture.

2.3 Cell culture

2.3.1 C2C12 cell culture in CP formulations

C2C12 mouse skeletal myoblasts were obtained from American Type Culture Collection (ATCC; LGC Standards, Teddington, United Kingdom) and cultured in DMEM containing 10% FBS (Cytiva, Marlborough, United States) and maintained 37°C in a humidified incubator with 5%

CO_2. Cells were passaged every 48 h to maintain confluence below 40%, unless otherwise specified. Recipient cells were seeded into a 6-well plate at a density of 3000 cells cm^{-2}, unless otherwise explicitly stated.

Differentiated myotube cultures were generated from C2C12 myoblasts seeded at 8000 cells cm^{-2} in DMEM supplemented with 10% FBS. Differentiation was induced by exchanging the bathing growth media for one consisting of DMEM supplemented with 2% horse serum on days 4 and 6. Analysis was performed on day 8, 4 days after the provision of differentiation media. To investigate the effect of pCM on the differentiation of myoblasts, donor myoblasts (2 days post-seeding) were resuspended in basal DMEM or CPS. Following PEMF exposures, the suspended myoblasts were allowed to condition the media for 1 h in a standard tissue culture incubator. Subsequently, the suspension was centrifuged at 1200 rpm for 5 min. The supernatant was supplemented with horse serum (200 µL) to a final concentration of 2% before being applied to recipient myoblast cultures (on day 4 of culture) in place of the standard differentiation medium. The same CM preparation and application were repeated on day 6 of culture.

Two paradigms were employed to generate CP formulations for the collection and testing of cell secretomes induced by PEMFs. In Paradigm 1, donor C2C12 cells were directly impregnated into CPGs upon polymerization. In Paradigm 2, donor cells were resuspended in CPSs (salt-deswelled CPG supernatant), prior to PEMF exposure.

For Paradigm 1, 75,000 cells mL^{-1} were dispersed in the CPG formulation in 15 mL conical tubes and exposed to PEMFs (0 mT or 1.5 mT) for 10 min, as outlined in Section 4.3.2. After stimulation, the donor cells were incubated at 37°C for an hour to condition the CPG. The cell-laden CPG was then centrifuged at 1200 rpm (~105 ×g) for 5 min to remove the cells, after which salt was introduced to trigger CPG deswelling as stated in Section 4.2.4. The deswelled CPG was removed by centrifugation at 10,000 ×g for 30 min, yielding cell- and CPG-free CM. The harvested CM was filtered and applied to recipient cell cultures 24 h post-seeding. For Paradigm 2, the salt-deswelled CPG supernatant (CPS) was prepared by adding the selected salt to the CPG, as described in Section 4.2.4. C2C12 cells were added at a concentration of 75,000 cells mL^{-1} to freshly prepared CPS in 15 mL conical tubes. Following PEMF exposure and conditioning within CPS, the resulting CM, obtained after donor cell removal, was filtered and applied to pre-plated C2C12 recipient cell cultures.

After 24 h of incubation, recipient cells in 6-well plates were harvested using TrypLE Express Enzyme (Thermo Fisher Scientific, Waltham, MA, United States) for enzymatic dissociation. Cell number was then determined via the standard trypan blue exclusion method and counted using a hemocytometer.

2.3.2 Pulsed electromagnetic field (PEMF) exposure

The PEMF signal used in this study has been previously described and characterized in the context of *in vitro* myogenesis [12,14,40]. Briefly, the PEMF devices produce spatially homogeneous, time-varying magnetic fields consisting of 20 × 150 μs on-off pulses for 6 ms at a repetition rate of 50 Hz. The magnetic flux density plateaued at a predetermined amplitude of 1.5 mT within ~50 ms (~17 T s^{-1}). All tissue culture flasks, dishes or tubes were placed within a region of greatest magnetic field uniformity wherein the entirety of the vessel is evenly exposed to the traversing magnetic field lines [12,41]. All PEMF-treated samples were compared with time-matched control samples (0 mT) that were manipulated in the same way as the experimental samples, including placement into the PEMF-generating apparatus for the designated time, except that the apparatus was not set to generate a magnetic field. All magnetically-stimulated samples were exposed once for a duration of 10 min to 1.5 mT amplitude PEMFs. CM containing no added CP were used as control cases for both 0 mT (cCM) and 1.5 mT (pCM) scenarios.

2.3.3 Western blot analysis of whole cell lysates

Protein extraction was performed using RIPA lysis buffer containing 50 mM NaCl, 1 mM EDTA, 50 mM Tris-HCl, 1% Triton X-100, 0.05% SDS, EDTA-free 1X protease inhibitor cocktail (Nacalai Tesque Inc., Japan), 1X PhosSTOP™ phosphatase inhibitor (Merck, Germany) and 0.1% sodium deoxycholate (Merck, Germany). Whole-cell lysates were collected using a cell scraper, incubated at 4°C for 30 min, then spun at 12,000 rpm for 15 min at 4°C. Protein concentration was determined using Pierce BCA Protein Assay Kit (Thermo Fisher Scientific, Waltham, MA, USA). Protein samples were prepared in 4X Laemmli buffer containing β-mercaptoethanol (Bio-Rad Laboratories and Sigma Life Science, USA, respectively) and denatured at 95°C for 5 min. 20–25 μg of protein was resolved by denaturing and reducing SDS-PAGE and subsequently transferred

to a PVDF membrane (Thermo Fisher Scientific, Waltham, MA, USA). Membranes were probed with primary antibodies as specified in Table S1 and were visualized using SuperSignal™ West Pico PLUS Chemiluminescent Substrate (Thermo Fisher Scientific) on LI-COR Odyssey Fc Imaging System.

2.3.4 Stability of CM and EVs in CPS

The stability of the PEMF-induced secretome in CPS was evaluated by measuring recipient-cell proliferation after storage and subsequent provision of CM and EVs. Basal DMEM and DMEM supplemented with 10% FBS served as controls.

PEMF-induced CM in CPS from Paradigm 2 were prepared as described in Section 4.3.1 and stored at 37°C for 2 and 6 h. Following storage, the CM was applied to pre-plated recipient cells, and cell enumeration was performed using the Trypan Blue assay after 24 h of incubation. EVs were also isolated from PEMF-induced CM in CPS via ultracentrifugation at 120,000 ×g for 2 h at 4°C using Quick-Seal Round-Top ultracentrifuge tubes on an Optima XPN-100 Ultracentrifuge (Beckman Coulter, USA). The isolated EVs were resuspended in CPS, stored at 4°C for 24 h, and subsequently applied to pre-plated recipient cells. Cell enumeration was performed 24 h later.

For physical characterization, the size distribution and concentrations of isolated EVs were determined using Nanoparticle Tracking Analysis (NTA) on a NanoSight LM10HSF (Nanosight Ltd., UK). For each sample, three replicate videos were captured and analyzed with the camera level set to 14.

2.3.5 Statistical analysis

All statistical analyses were performed using GraphPad Prism (Version 10.5.0) software. One-way analysis of variance (ANOVA) was employed to compare values across two or more groups, supported by Sidak's multiple comparisons test.

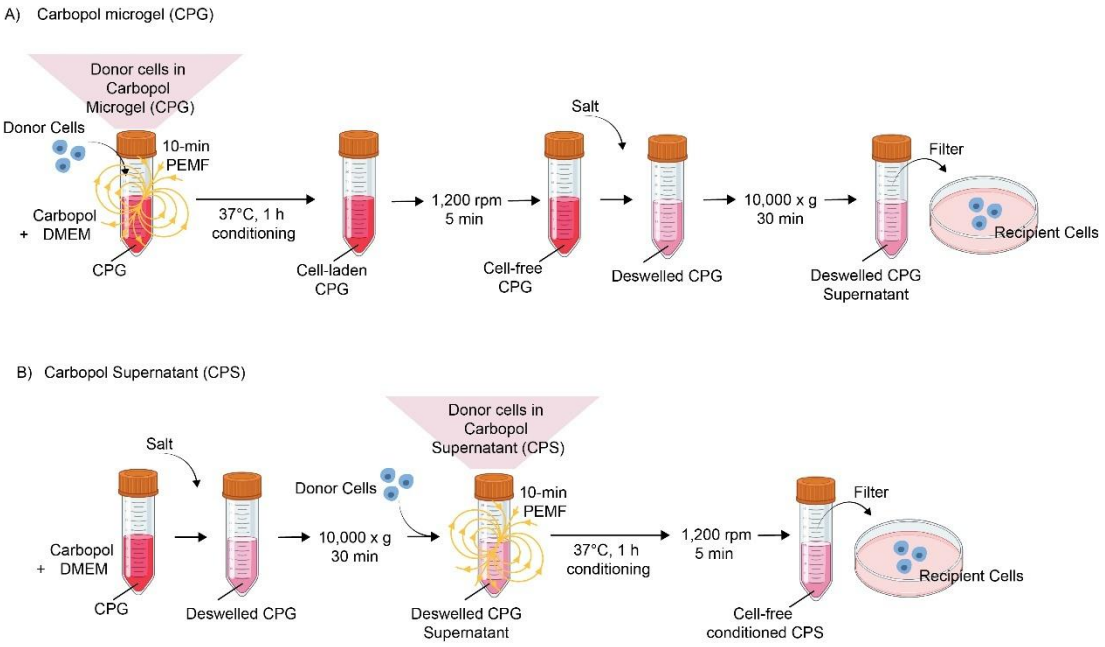
3. Results

3.1 Concept and characterization of media formulations

The acronyms and the corresponding descriptions of the media formulations referenced throughout this article are as follows:

- CPG (Carbopol® microgel): Carbopol polymer formulated in basal media.
- CPS (Carbopol supernatant): The media solution remaining after centrifugation of salt-deswelled CPG and used either as a conditioning medium or secretome stabilizer.
- cCM (Control conditioned media): Media conditioned in the absence of Carbopol polymers and without PEMF exposure (0 mT) to the secretome donor cells.
- pCM (PEMF-conditioned media): Media conditioned in the absence of Carbopol in conjunction with exposure of the secretome donor cells to 1.5 mT PEMFs for 10 min.

Diverse CP formulations were evaluated for their ability to enhance the potency and stability of PEMF-induced cell secretomes. Two principal hypotheses were explored: (A) whether the 3D microenvironment conferred by a CPG, by providing a structurally supportive biomimetic environment, could enhance secretome bioactivity, and; (B) whether remnant CP polymers resulting from CPG deswelling with salts could improve the stability of the cell-secreted factors (Figure 1).



286

287 **Figure 1 Schematic of PEMF-induced cell secretome paradigms and workflow.** (A) Paradigm
288 1: Donor cells were directly impregnated into CPG and exposed to PEMFs, whereas in (B)
289 Paradigm 2: Donor cells were suspended in salt-deswelled CPS prior to PEMF stimulation. Final
290 CM was provisioned to recipient cells for testing and analysis.

291

292 With reference to the first hypothesis, to create confined spaces for entrapping and suspending
293 donor cells along with their secreted agents, we sought to determine the critical polymer
294 concentration for the formation of a microstructurally jammed media suspension, determined by
295 the emergence of a yield stress capable of keeping cells suspended in media [42]. Approximating
296 the cells as spheres, the characteristic yield stress (σ_Y) can be estimated based on the reported
297 densities of cells and basal media (Equation 2) [28,43]:

$$\sigma_Y \geq \frac{1}{3}\Delta\rho g d \qquad \textbf{Equation 2}$$

$$\sigma_Y \geq \sim 0.03\ Pa$$

298

299 where $\Delta\rho$ is the density difference between the cell (1100 kg m^{-3}) and basal media (1010 kg m^{-3}),
300 g is the gravitational acceleration constant and d is the approximate diameter of the cells of interest
301 (10^{-4} m). We note that this analysis assumes the microgel suspension behaves as a continuum,

which is unlikely at the cell length scale. Therefore, we use this characteristic yield stress as a lower bound, and for cell-suspension media, we utilize a polymer concentration of at least 0.8%, which yields a yield stress an order of magnitude higher than the calculated value.

Rheological analyses indicated that the CP concentrations at 0.8% ($\sigma_Y{}^{HB}$: 0.27 ± 0.01 Pa) and 1% ($\sigma_Y{}^{HB}$: 2.77 ± 0.17 Pa) exhibited yield stress behavior (Figure 2A). Meanwhile, the 0.6% CP formulation showed no measurable yield stress, indicating that the volume fraction of the microgels at this concentration is insufficient to pack and jam against one another. These rheological results aligned with microstructural observations (Figure 2B (insets) and Figure S1 (uncropped images)), which revealed a monotonic decrease in the average size of microgel aggregates (10 – 14 μm^2) with increasing polymer concentration (Figure 2B and Figure S2). This trend suggests that microgel aggregates at high packing fractions undergo greater compression with increasing concentration, consistent with a previously reported size reduction (~8 – 20%) for a CP polymer (0.25 – 1.25%) in water [44]. Given that the yield stress of the 0.8 and 1% CP media is at least 10 times higher than the characteristic minimum σ_Y required (~0.03 Pa) to suspend cells, donor cells were expected to remained stationary in suspension over the timescale of the relevant workflow.

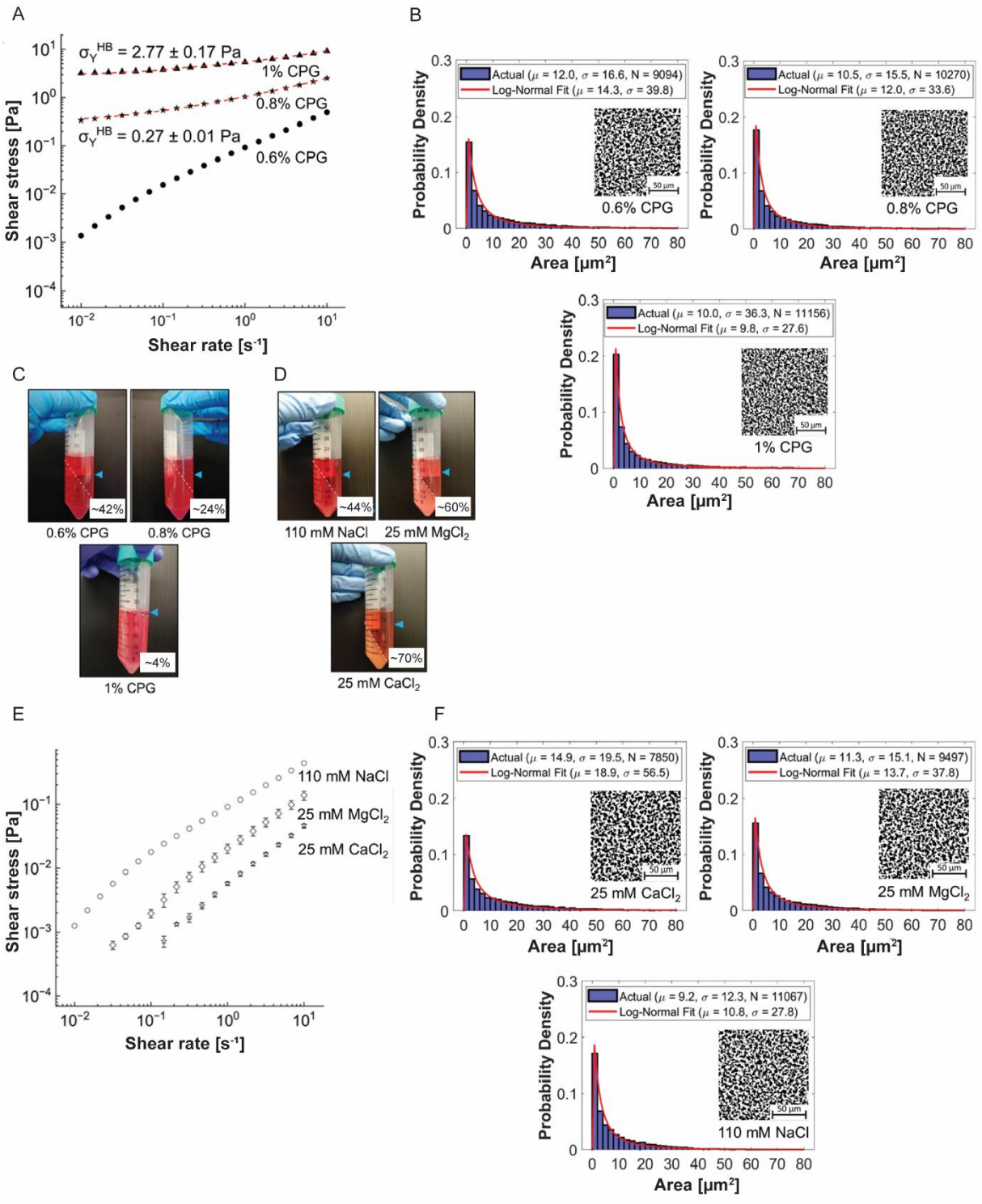


Figure 2 Characterization of CPG suspensions: Polymer concentration and ionic effects. (A) Rheological behavior of CPG suspensions at varying polymer concentrations (0.6 %, 0.8 %, and 1 %). A stress plateau at low shear rates indicates an apparent yield stress; the dashed line represents the Herschel-Bulkley yield-stress fit. Error bars smaller than the symbols are omitted.

(B) Probability density function of CPG aggregate areas ($n = 5$) with Log-normal distribution fits for each concentration. Inset: representative micrograph of CPG aggregates (40×). Full images are provided in the Figure S1. (C) CPS recovery efficiency after centrifugation for the same polymer concentrations. (D) CPS recovery efficiency for 0.8 % CPG with different salts and after centrifugation. (E) Rheological response of 0.8 % CPG after addition of different salts (sodium chloride (NaCl), calcium chloride ($CaCl_2$) and magnesium chloride ($MgCl_2$)). Error bars (standard deviation of three repeats) smaller than symbols are omitted. (F) Probability density function of CPG aggregate areas ($n = 5$) with Log-normal fits after salt addition. Inset: representative micrograph of aggregates (40×) (also Figure S1).

For correlation with effective secretome retrieval and cost-effectiveness for cell culture applications, CPS recovery percentage was assessed. The percentage recovery of CPS (~4–42%) decreased by ~20% with each 0.2% increment in polymer concentration from 0.6% to 1% (Figure 2C). This indicates a reduction in free space within the media, consistent with the observed rheological and morphological results. Considering both rheological and media recovery, a polymer concentration of 0.8% CP was chosen as the optimal formulation for further study, balancing CPS recovery and the σ_Y required to suspend cells.

3.2 Enhancement of media recovery by modulating the microgel degree of swelling

CP polymer microgels exhibit sensitivity to ion concentration, typically deswelling in response to higher ionic strengths [28,29,45,46]. By leveraging this property, we first sought to improve the CPS recovery by introducing salt following the conditioning phase by donor cells. Since NaCl is the predominant ionic species in tissue fluids, this approach is both physiologically relevant and applicable for cell culture applications as long as the pH remains within an acceptable range [47]. To maintain a pH of approximately 7.4 while reaching a sufficient recovery efficiency, we identified a final concentration of added NaCl of 110 mM to produce a workable sample volume, improving the percentage recovery of CPS volume by approximately ~2-fold (Recovery efficiency and pH as a function of added salt concentration shown in Figure S3).

The effects of the divalent salts, $CaCl_2$ and $MgCl_2$, on the deswelling of microgels were next explored. Complete media recovery was achieved with 50 mM $CaCl_2$ when tested across a range of salt concentrations (Figure S4), exceeding the ~80% recovery obtained with 1500 mM NaCl (Figure S3). To match the pH of CPS derived from NaCl, 25 mM of $CaCl_2$ was chosen, yielding 70% recovery in subsequent experiments. Similarly, 25 mM of $MgCl_2$ enhanced media recovery, although the effect was less pronounced that achieved with $CaCl_2$ (~60%, Figure 2D).

Upon incorporating salt, rheological characterization revealed a transition of the CP media from a yield-stress (jammed) to a non-yield-stress (unjammed) state, which can be linked to reduced microgel volume fraction and packing due to microgel deswelling (Figure 2E). The microgel packing was lowest in CP media incorporated with $CaCl_2$, followed by $MgCl_2$ and NaCl. This trend aligns with the media recovery results, where reduced microgel packing corresponded to increased media recovery. Notably, microscopic analysis showed that the addition of $CaCl_2$ (19 ± 57 μm^2) and $MgCl_2$ (14 ± 38 μm^2) resulted in larger microgel aggregates as compared to both the control and NaCl (11 ± 28 μm^2) (Figure 2B, 2F; Figure S1, S2). The mechanism by which microgels deswell upon the addition of NaCl is likely via a shielding effect of the salt ions, which would reduce the electrostatic repulsive forces between negatively charged carboxyl groups along the CP polymer backbone (Figure S5) [48,49]. In contrast, the bigger aggregates formed with $CaCl_2$ and $MgCl_2$ may be attributed to the formation of polymeric complexes. Divalent calcium ions likely form complexes with carboxylic acid groups on two CP polymer surfaces, similarly to complexes formed in other polyelectrolyte systems reported [45,50–52]. These calcium-carboxylate complexes are expected to exhibit hydrophobic character that serves to reduce water bonding and lead to less swelling of the microgel. Meanwhile, magnesium cations may bind more weakly to carboxylate groups due to their stronger hydration, which would hinder effective interaction with the CP polymer [53]. That is, magnesium cations would tend to form solvent-shared ion pairs with carboxylate groups, while calcium cations would form direct contact ion pairs.

3.3 Comparative bioactivity of CP formulations

Subsequent cell culture experiments were performed using the optimized CP concentration of 0.8%. To better understand how the degree of CP swelling and microstructural packing might

affect the bioactivity of donor cell secretome, we compared the proliferative response of cells which were conferred the CM harvested from PEMF-stimulated cells in CPG versus CM obtained from cells stimulated by PEMFs while in CPS. The recipient cellular proliferative responses obtained with the distinctly CM were compared to that obtained with tissue culture media supplemented with 10% FBS (grey bar), which is commonly employed in standard tissue culture procedures. In Paradigm 1, cells impregnated within CPGs were stimulated by PEMFs (10 min) wherein conditioning occurred before deswelling and the collection of CM (Figure 1). In Paradigm 2, cells in CPS were stimulated by PEMFs wherein conditioning occurred immediately before provision to recipient cells. In both scenarios, cells were allowed to condition their respective Carbopol-based environments (CPS or CPG) for 60 min, and the final donor-cell-conditioned CPS was prepared using 25 mM $CaCl_2$ before being provided to recipient cells for growth analysis. The results presented in Figure 3A indicate that pCM from CPS elicited the greatest proliferative response in recipient cells compared with pCM from CPG. Notably, proliferation in the CPS scenario was comparable to that measured in FBS-supplemented DMEM. We therefore conclude that the enhanced proliferation of recipient cells following the provision of PEMF-induced secretomes is predominantly due to the conveyance of soluble factors rather than the molecular crowding afforded by CP per se. The general trend of improved outcomes for CPS versus CPG was confirmed for 0.6% and 1% formulations (Figure S6). As a result, for the remaining investigations, we opted to focus on the performance of the CPS system obtained from 0.8% CPG.

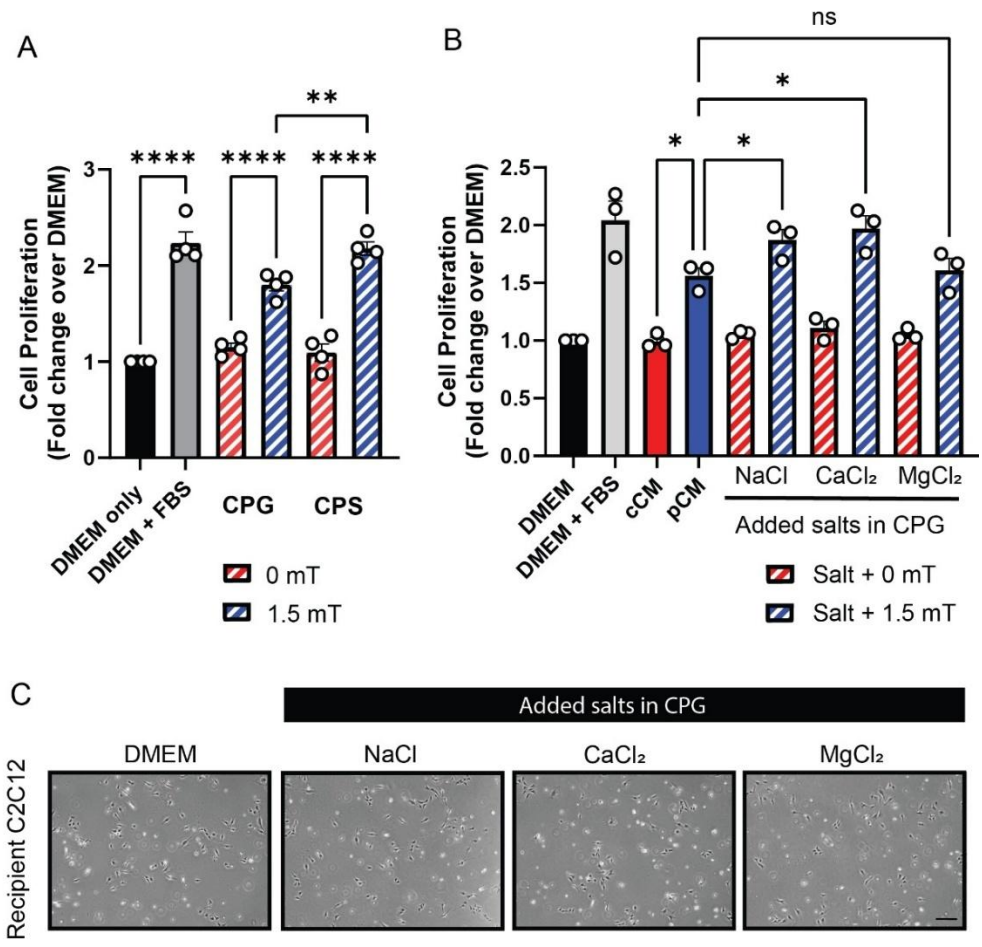


Figure 3 Comparative bioactivity of PEMF-induced secretomes from different CP formulations. (A) CPS versus CPG conditioning efficiency. Recipient cell proliferation in response to CM generated from donor cells treated in either 0.8% CPG or CPS. Donor cells were either embedded in CPG or suspended in fresh CPS prior to PEMF exposure. Both media were deswelled using 25 mM $CaCl_2$. (B) Salt-specific effects on CPS potency. Recipient cell proliferation (24 h) after provision of PEMF-conditioned media (pCM) in DMEM or pCM generated from CPS using various salts (110 mM NaCl, 25 mM $CaCl_2$, 25 mM $MgCl_2$). (C) Representative phase contrast micrographs of recipient C2C12 cells after provision of DMEM or CPG deswelled using different salts (scale bar = 200 µm). Data in (A) and (B) are expressed as fold change over basal DMEM and represent mean ± SEM of n = 3-4 biological replicates (white dots) with *$p < 0.05$, **$p < 0.01$ and ****$p < 0.0001$.

3.4 Effects of different ionic species on cellular protein expression

Protein expression analysis was performed on recipient cells receiving CM from donor cells resuspended in CPS (Figure 1, Paradigm 2). Figure 3B depicts the proliferation of C2C12 recipient cells 24 h after the provision of different CMs, compared to cells cultured in basal media or FBS-supplemented DMEM. PEMF exposure (1.5 mT) consistently enhanced the potency of PEMF-induced CM (pCM), particularly with CPS generated from deswelled CPGs using NaCl and $CaCl_2$, yielding proliferative levels comparable to those observed with FBS-supplemented DMEM. pCM from deswelled CPG using $MgCl_2$, however, did not surpass the pCM derived in DMEM alone. Furthermore, the morphology of recipient cells cultured in the various CPS was similar to that of cells cultured in basal DMEM (Figure 3C), suggesting comparable biocompatibility. Western blot analysis revealed that pCM in DMEM, or pCM generated from CPG deswelled using NaCl and $CaCl_2$, preferentially upregulated Cyclin D1 and Cyclin B1 (Figure 4, panels A and B), which are key regulators of myoblast expansion in response to direct PEMF exposure [54]. Conversely, $MgCl_2$ showed no change.

Non-significant, yet consistent trends were observed in the expression levels of other key proteins. For instance, p21, which inhibits myoblast proliferation [55], showed a tendency to be relatively higher in cells provided pCM generated in NaCl-deswelled CPGs or basic pCM. In contrast, pCM from $CaCl_2$-deswelled CPGs decreased p21 expression relative to its respective cCM (Figure 4C), consistent with the greatest elevation in cyclin D1 expression and stimulation of cell proliferation in $CaCl_2$-deswelled CPGs. Phosphorylated ERK (extracellular signal-regulated kinase), a negative regulator of myoblast differentiation [56], was the least relatively depressed in recipient myoblasts given $MgCl_2$-deswelled CPGs (Figure 4D), consistent with the smallest proliferative response among the various comparisons. Accordingly, phosphorylated JNK (c-Jun N-terminal kinase), a mediator of stress-induced cell death [57] was most highly elevated in cells treated with $MgCl_2$-deswelled CPGs, particularly in the unexposed (cCM) conditions (Figure 4E), indicating that there was some level of cytotoxicity associated with the usage of $MgCl_2$. On the other hand, the overall lowest levels of phospho-JNK protein expression were observed in recipient myoblasts that had been provisioned with PEMF-exposed $CaCl_2$-deswelled CPGs (pCM). Less defined trends were observed for TRPC1 expression, a key regulator of myoblast proliferation, migration, and differentiation [58] (Figure 4F), though levels of TRPC1 tended to be highest in cells treated with

secretomes harvested from PEMF-exposed $CaCl_2$-deswelled CPGs (pCM). These findings indicate that the ionic species used to deswell the CPGs influenced the bioactivity of the resulting CM on recipient cells in culture, with $CaCl_2$ and $MgCl_2$ yielding the most and least favourable cellular profiles, respectively.

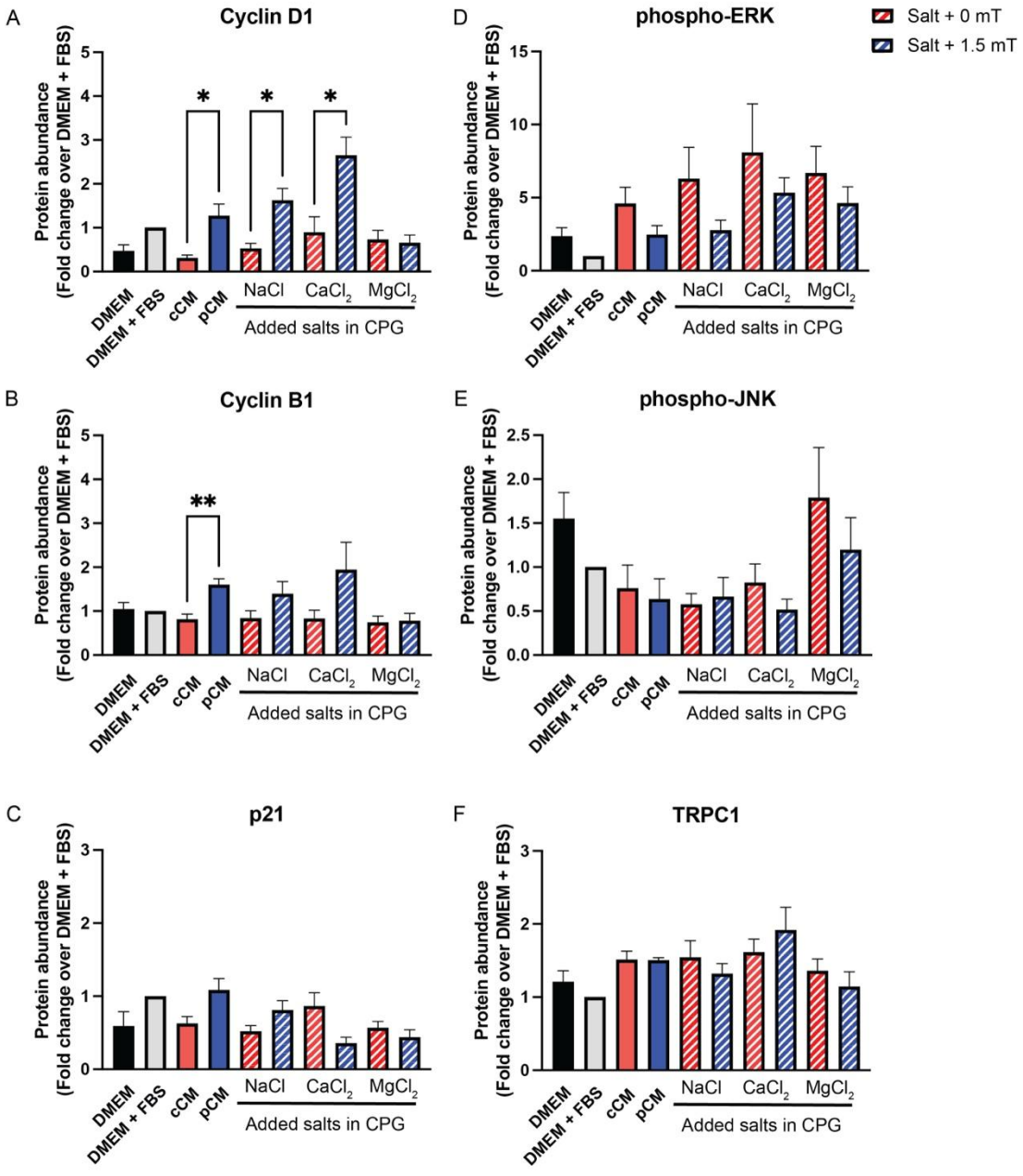


Figure 4 Protein expression of recipient cells in response PEMF-induced CM in salt-deswelled CPG. Bar charts showing the relative protein abundance (expressed as fold change over

cells treated with DMEM + FBS) of (A) Cyclin D1, (B) Cyclin B1, (C) p21, (D) phospho-ERK, (E) phospho-JNK and (F) TRPC1. The data represent the average of $n = 6$ biological replicates. The error bars represent the standard error of the mean, with * $p<0.05$ and ** $p<0.01$.

3.5 CPS preserves the bioactivity of CM and EVs during storage

The potency and stability of CM and EVs in CPS after storage was next compared. To this end, CPSs derived via $CaCl_2$ addition were either provided to donor cells for the generation of crude CM or used for the resuspension of isolated EVs. Basic PEMF-stimulated CM (pCM without CPS) (Figure 5A, blue bar), promoted recipient cell growth to a comparable degree as FBS-supplemented DMEM. On the other hand, pCM generated in CPS (hatched blue) exhibited an enhancement in the proliferation of recipient cells that surpassed that of FBS-supplemented DMEM (Figure 5A) as well as retained potency up to 6 h at 37°C, as evidenced by no significant loss of bioactivity between timepoints. Furthermore, PEMF-induced EVs demonstrated proliferative efficacy comparable to FBS-supplemented media (Figure 5B, blue bar) and moreover, retained bioactivity after 24 h of storage at 4°C when stored in CPS (Figure 5B, hatched blue bar). By contrast, unprotected EVs that were resuspended in naïve DMEM (second blue bar) lost efficacy under similar storage conditions. These findings underscore the protective effect of CPS in preserving the bioactivity and stability of secretome components.

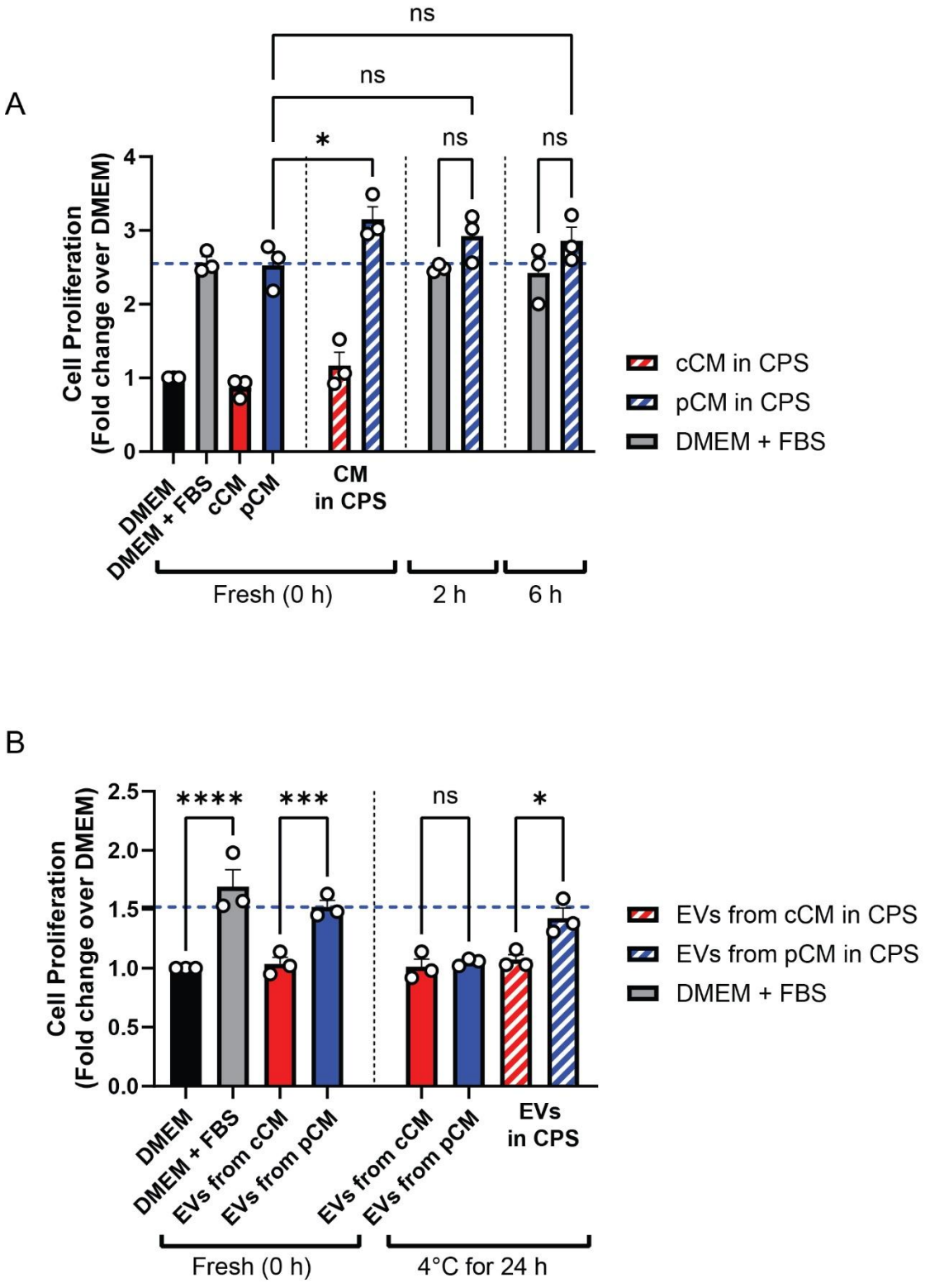


Figure 5 CPS preserves the bioactivity and stability of CM and EVs for extended storage. (A) Recipient cell proliferation after treatment with CM stored at 37°C for 0, 2, or 6 h. (B)

Recipient cell proliferation after treatment with EVs stored at 4°C for 24 h. Blue lines indicate the fold-change of recipient cell proliferation achieved by PEMF-stimulated CM (pCM without CPS) or PEMF-stimulated EVs isolated and resuspended in DMEM (first blue bar). Data represent the average of $n = 3$ biological replicates (white dots), with 3 technical replicates each. The error bars represent the standard error of the mean with * $p<0.05$, *** $p<0.001$ and **** $p<0.0001$.

3.6 CPS-stabilized pCM promotes myogenic differentiation

Protein markers of myogenic differentiation were upregulated in myoblast cultures following provision of either basic pCM or CPS pCM. Provocatively, the conditioning of CPS by myoblasts in suspension that had been exposed to PEMFs and then administered to myoblasts in the form of differentiation media (supplemented with 2% Horse Serum) (Figure 6) upregulated the expression of proteins characteristic of late myogenic differentiation *in vitro* (Desmin and MyoG), while reducing the expression of proteins responsible for early myogenic differentiation (MyoD) and proliferation (Cyclin D1 and Cyclin B1) relative to unconditioned DMEM. These results show that pCM in CPS promoted myoblast differentiation at the expense of proliferation.

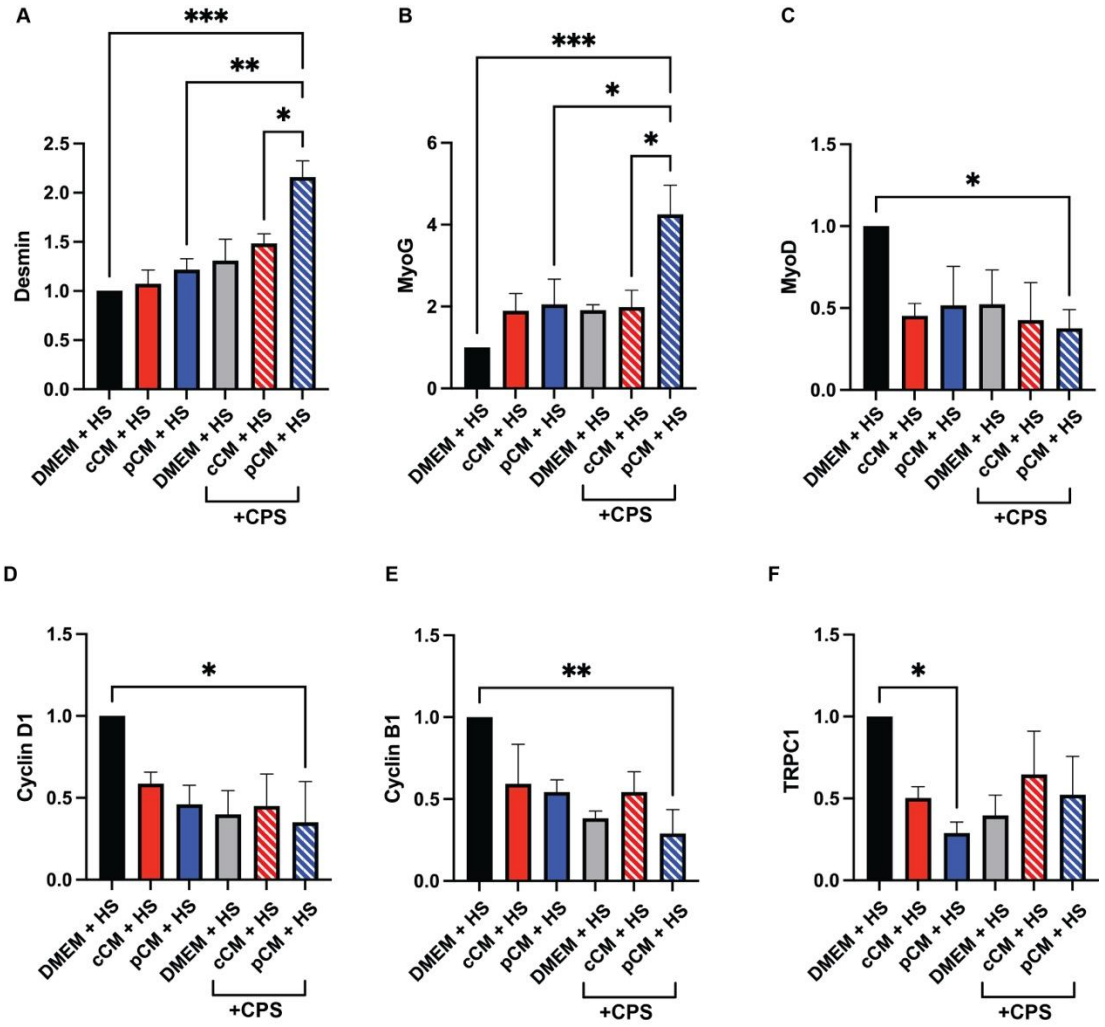


Figure 6 CM from PEMF-stimulated myoblasts in CPS enhances myogenic differentiation. CM were collected from PEMF-stimulated myoblasts suspended in CPS, supplemented with 2% horse serum (HS), and administered on days 4 and 6 of differentiation. Differentiation was assessed on day 8. The bar charts show the relative protein expression of (A) Desmin, (B) MyoG, (C) MyoD, (D) cyclin D1, (E) cyclin B1, and (F) TRPC1. Data are expressed as fold change relative to the DMEM + HS control for each target protein and represent the mean of $n = 3$ biological replicates. The error bars represent the standard error of the mean with * $p<0.05$, ** $p<0.01$, *** $p<0.001$ and **** $p<0.0001$.

Conversely, the administration of magnetically CM harvested from differentiated myotubes exposed in the presence of CPS (without horse serum) promoted the differentiation of proliferating

myoblasts and forestalled proliferation (Figure 7) to a greater degree and more comprehensively than from CPS secretomes collected from myoblasts.

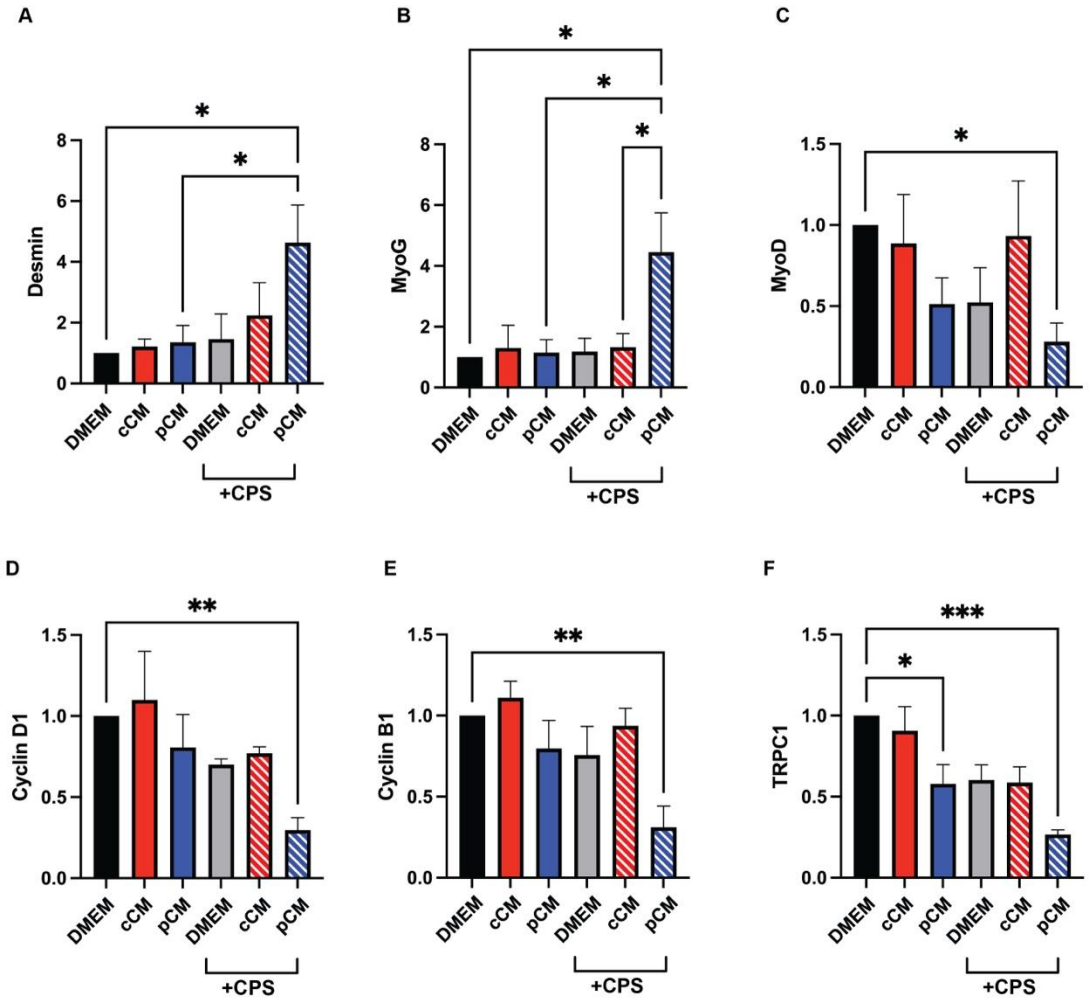
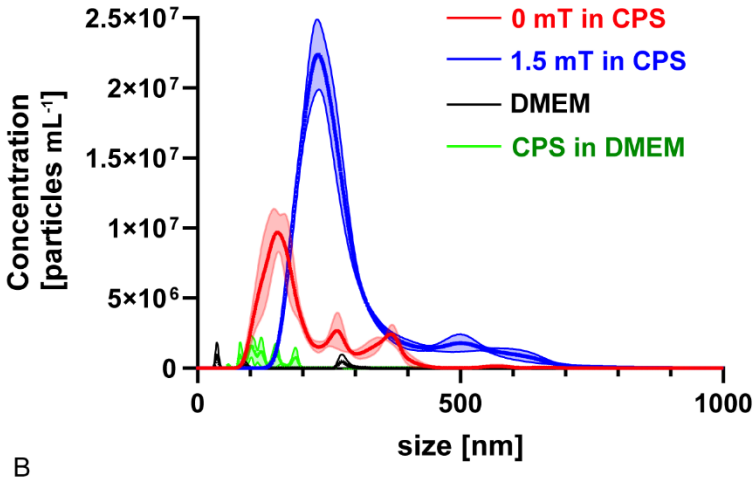


Figure 7 CM from PEMF-stimulated myotubes in CPS promote myogenic differentiation. pCM were collected from PEMF-stimulated myotubes in CPS and administered to proliferating myoblast cultures to assess paracrine effects on differentiation 24 h later. Bar charts show the relative protein expression of (A) Desmin, (B) MyoG, (C) MyoD, (D) Cyclin D1, (E) Cyclin B1, and (F) TRPC1. Data are expressed as fold change relative to the respective control (DMEM) for each target and represent the mean of 3 biological replicates. The error bars represent the standard error of the mean with * $p<0.05$, ** $p<0.01$, and *** $p<0.001$.

3.7 PEMF enhances EV yield and size in a stabilizing CPS

It has previously been shown that PEMF exposure increases the number and size of extracellular vesicles released [12]. Quantitative nanoparticle tracking analysis (NTA) of conditioned samples revealed that exposure of myoblasts to 1.5 mT PEMFs while in CPS produced a clear increase in EV number and size relative to unexposed samples (Figure 8, panels A and B). The concentration of vesicle-sized particles increased approximately 2.6-fold, from 1.08 (± 0.13) × 10^9 particles mL^{-1} in unstimulated controls (0 mT) to 2.84 (± 0.11) × 10^9 particles mL^{-1} following PEMF stimulation. Additionally, the mean particle diameter increased from 207.4 (± 9.4) nm to 283.1 (± 1.6) nm, and the modal size (the most frequent diameter) increased from 153 (± 8.4) nm to 237.1 (± 7.7) nm. This shift was evident across the entire size distribution, as indicated by significant increases in D10, D50 (median), and D90 (Figure 8B). By contrast, NTA of control media confirmed that fresh DMEM and acellular CPS exhibited negligible background particles. These data demonstrate that PEMF stimulation within CPS not only enhances EV secretion from myoblasts but also promotes the release of a vesicle population with a larger median size [12].

A



B

Concentration	0 mT in CPS	1.5 mT in CPS	*Significance*	DMEM	CPS in DMEM
Particles mL^{-1}	1.08 ± 0.13 x 10^9	2.84 ± 0.11 x 10^9	*t*-test ($p < 0.05$)	2.49 ± 1.67 x 10^7	8.09 ± 1.47 x 10^7
Size Data					
Mean	207.4 ± 9.4	283.1 ± 1.6	yes	123.7 ± 34.0	130.6 ± 2.2
Mode	153 ± 8.4	237.1 ± 7.7	yes	71.2 ± 17.2	103.2 ± 11.7
SD	91.3 ± 8.9	111.8 ± 3.2	no	45.7 ± 36.6	48.8 ± 4.9
D10	121.3 ± 5.8	189.5 ± 1.9	yes	63.2 ± 14.4	97.8 ± 9.5
D50	173.9 ± 10.7	246.6 ± 3.0	yes	148.9 ± 60.5	112.9 ± 6.0
D90	354.1 ± 12.5	460.5 ± 18.7	yes	165.2 ± 64.8	165.7 ± 12.3

Figure 8 PEMF enhances EV secretion and size in CPS. (A) NTA histograms showing EVs from myoblasts under the indicated conditions: unstimulated (0 mT, red) or stimulated (1.5 mT, blue) in CPS. Background controls for DMEM (black) and CPS in DMEM (green) are shown. (B) Quantitative summary of the average concentration and size data (± standard error) generated from n=3. Statistical significance was determined using an unpaired two-tailed Student's *t*-test.

4. Discussion and Conclusions

The cell secretome offers significant advantages over traditional cell-based therapies, including lower immunogenicity and easier production, handling, and storage. We demonstrated that although both CPG and CPS significantly improved the proliferative potential, differentiation capacity, and stability of PEMF-induced cellular secretomes, differences were implied in their modes of action. The liquid supernatant (CPS) recovered after salt deswelling of a CPG was more effective and protective as a conditioning medium than the microenvironment provided by a CPG

per se (Figure 3). This finding shifted the focus of this study away from the manner in which CPG-associated molecular confinement supports secretome collection to the role of deswelled CP residues in CPS stabilization, representing an important step towards cleaner and more potent secretome technologies for clinical exploitation. We proposed that the enhanced bioactivity of the liquid supernatant is mediated by residual CP polymers remaining in the salt-deswelled CPS. Dynamic light scattering analyses of acellular CPS confirmed the presence of colloidal particles between ~20 and ~200 nm that were not present in basal media (Figure S7). Notably, salt-deswelled CPS displayed a broader distribution of intermediate particle sizes compared to CPS without added salt, indicating ionic modification of the CP residues. Although CP polymers are negatively charged due to their anionic carboxylate functional groups [59,60], zeta potential measurements revealed that these CP residues carried a net positive surface charge in the media (Figure S8). This charge reversal is likely attributable to the complexation of CP carboxylate groups with cationic components of the DMEM, which mask their native negative charge. These residual complexes demonstrated excellent colloidal stability, maintaining a consistent size and surface charge over seven days of storage (Figure S8 and S9). We posit that these positively charged residues, by preventing the aggregation of anionic secretome components, shielded them from thermodynamic degradation, thereby mimicking natural stabilizers and paralleling other synthetic strategies whereby engineered polyelectrolyte complexes preserved EV integrity and function [61]. While factors such as pH and ionic strength are known to influence the stability of secretome components [62], our data confirmed that the CP residues within CPS provide a stabilizing milieu that maintains the myogenic efficacy of both CM and isolated EVs, yet with a minimum amount of exogenous stabilizing CP.

The ionic species used for the deswelling of CPGs also influenced the bioactivity of the resultant CPS. Specifically, deswelling the CPGs with $CaCl_2$ produced the most favourable cell-cycle and stress-signalling secretome profiles, whereas CPG deswelling with $MgCl_2$ produced the least favourable profiles as well as produced an apparently cytotoxic secretome (Figure 3 and Figure 4). The presented CP system hence reveals a high level of tunability for achieving diverse developmental outcomes. The CPS platform would be also compatible with other biophysical induction platforms. PEMF paradigms constitute an emerging class of biophysical stimulation methods for inducing cell secretomes [12,18,63]. The translational appeal of PEMF modalities lies in their non-invasive, contactless, and readily scalable manner of delivery, which aligns well with

clinical and biomanufacturing requirements. Magnetically stimulated pCM could stimulate either the proliferation or differentiation of recipient cells, depending on the developmental status of the donor cells (Figure 6 and Figure 7), underscoring its adaptability for diverse regenerative applications. For instance, the secretome-mediated transference of cellular phenotype from donor to recipient cells could potentially extend to metabolic and inflammatory statuses, reminiscent of the Senescence-Associated Secretory Phenotype (SASP) and its potential clinical exploitation for provoking senescence in cancer [64]. The presented CPS workflow provides a template for optimizing the recovery as well as preserving the bioactivity of the cell secretome. The secretome enhancement demonstrated in the present study arose from a combination of both complementary methods: (1) an increased secretome induction driven by brief PEMF exposure, and; (2) an enhanced stabilization of magnetically-released secretome factors by the engineered CPS media.

The capacity of PEMF exposure to act as a secretome inducer lies in its ability to modulate mitochondrial function, a crucial convergence point for several described cellular secretion pathways [15,16]. Similarly to secretome induction by hypoxia [65], PEMF exposure transiently alters mitochondrial activity, calcium flux, and reactive oxygen species (ROS) signalling [14,41]. On the other hand, PEMF exposure systems can be engineered to be highly localizable and to deliver a mild form of mitohormetic eustress that gently primes mitochondrial respiration without necessarily inducing mitochondrial dysfunction [41]. The controlled bioenergetic tuning afforded by PEMF exposure allows the platform to promote the release of a therapeutically programmed secretome [12,17,18,66].

Exosome therapy is an advantageous alternative to whole-cell therapies, particularly when stem cell integration is not necessary [67]. As cell-surrogates, EVs, including exosomes, replicate many of the regenerative and immunomodulatory effects of whole-cell therapies while offering superior safety profiles, including lower immunogenicity, minimal tumorigenic potential, and potential logistical benefits such off-the-shelf deployment [67]. The widespread therapeutic translation of EVs, however, hinges on addressing two challenges: (1) scalable production of functionally enhanced EVs and (2) preservation of their bioactivity during storage and transport [68].

PEMF modalities represent a non-invasive biophysical tool kit with which to address the first challenge. By acting as a natural and non-invasive form of mitohormetic stimulation [41], PEMF stimulation modulates the cell secretome response [12,17,69–71] and in doing so, enhances both

the quantity and regenerative potential of EV output [12,72,73]. Studies across diverse cell types confirm that PEMF exposure increases the quantity of EVs released [72,73] as well as modifies their physical characteristics, such as an increase in mean vesicle size [12]. Provocatively, a recent study has shown that EVs containing mitochondria increase in number and size upon magnetic field exposure that are capable of ameliorating intervertebral disc degeneration [74]. Other studies have further substantiated that PEMF exposure functionally "preconditions" donor cells to enrich EV cargo with pro-regenerative factors to ultimately enhance outcomes in models of muscle, bone, cartilage, and nerve repair [12,72,75,76]. These findings position PEMFs as a scalable bioreactor-compatible technology for producing EVs with tailored therapeutic profiles.

This present study also directly addressed the practical challenge of improving secretome stability. The therapeutic potential of EVs is compromised by their rapid degradation upon release into basal saline solutions. Here, we introduce CPS as a stabilizing milieu that maintains secretome bioavailability in both CM and isolated EVs during storage, a protective effect not afforded by standard culture media. Therefore, integrating PEMF exposure to enhance EV production and CPS for post-production stabilization lays the foundation for a cohesive biomanufacturing strategy. This synergy enables the harvest and stabilization of EV-rich CM into a standardized, clinically viable, off-the-shelf therapeutic product.

CP media formulations, particularly in the form of salt-deswelled CPS, represent a versatile and safe platform for enhancing secretome-based therapies. The system is highly tuneable, synergistic with biophysical means of secretome induction, and effective at preserving cellular secretome bioactivity. Future studies are warranted explore its compatibility with other cell types and inductive stimuli, elucidate the molecular interactions underlying CP-secretome stabilization in greater depth, and investigate long-term culture performance. The presented integrated approach helps bring the regenerative medicine industry one step closer to realizing the full clinical potential of engineered cellular secretomes and EV therapies.

Data Availability

All data supporting the findings of this study are available within the paper and its Supplementary Information.

Acknowledgements

LCW and CJKW contributed equally to this work. The authors thank Dr. Ariel Chua from the Singapore-MIT Alliance for Research and Technology Centre for assistance with the characterisation of particle size distributions of CP aggregates. The National University of Singapore has filed a patent application based on the research in this study. This study was funded by the National Research Foundation, Singapore and the Agency for Science, Technology and Research (A*STAR) under the Singapore Food Story R&D Programme (Grant No. W23W2D0010). The funder played no role in study design, data collection, analysis and interpretation of data, or the writing of this manuscript.

CRediT Author Statement

Conceptualization: RAJ, AF-O, AZN; Methodology: LCW, CJKW; Investigation: LCW, CJKW, KYW, SMEC; Writing – Original Draft: LCW; Writing – Review & Editing: YKT, AF-O, AZN; Visualization: LCW, CJKW, KYW, SMEC, YKT; Supervision: RAJ, AF-O, AZN; Funding acquisition: RAJ, AF-O, AZN. All authors reviewed the manuscript.

Declaration of Competing Interest

Author AF-O reports being a contributor to QuantumTx Pte. Ltd., which elaborates electromagnetic field devices for human use. Author AF-O is an inventor on patent WO 2019/17863 A1, System and Method for Applying Pulsed Electromagnetic Fields. Authors AF-O, CJKW, YKT, and RAJ are inventors on patent WO 2024/005714 A1, Directionally-specific Magnetic Modulation of the Cell Secretome for Medical and Commercial Applications. All Authors are inventors on patent WO/2025/212041, Collapsible cell-encapsulating scaffolds to enhance magnetically-induced secretome stabilisation and potency. There are no other known competing financial interests or personal relationships that could have appeared to influence the work reported in this paper.

Declaration of generative AI and AI-assisted technologies in the writing process

During the preparation of this work the authors used ChatGPT in order to improve readability. After using this tool/service, the authors reviewed and edited the content as needed and take full responsibility for the content of the publication.

References

[1] L. Daneshmandi, S. Shah, T. Jafari, M. Bhattacharjee, D. Momah, N. Saveh-Shemshaki, K.W.-H. Lo, C.T. Laurencin, Emergence of the stem cell secretome in regenerative engineering, Trends Biotechnol. 38 (2020) 1373–1384. https://doi.org/10.1016/j.tibtech.2020.04.013.

[2] K. Da Silva, P. Kumar, Y.E. Choonara, The paradigm of stem cell secretome in tissue repair and regeneration: Present and future perspectives, Wound Repair and Regeneration 33 (2025) e13251. https://doi.org/https://doi.org/10.1111/wrr.13251.

[3] R. Mitchell, B. Mellows, J. Sheard, M. Antonioli, O. Kretz, D. Chambers, M.-T. Zeuner, J.E. Tomkins, B. Denecke, L. Musante, B. Joch, F. Debacq-Chainiaux, H. Holthofer, S. Ray, T.B. Huber, J. Dengjel, P. De Coppi, D. Widera, K. Patel, Secretome of adipose-derived mesenchymal stem cells promotes skeletal muscle regeneration through synergistic action of extracellular vesicle cargo and soluble proteins, Stem Cell Res. Ther. 10 (2019) 116. https://doi.org/10.1186/s13287-019-1213-1.

[4] J.P. Bost, O. Saher, D. Hagey, D.R. Mamand, X. Liang, W. Zheng, G. Corso, O. Gustafsson, A. Görgens, C.I.E. Smith, R. Zain, S. El Andaloussi, D. Gupta, Growth media conditions influence the secretion route and release levels of engineered extracellular Vesicles, Adv. Healthc. Mater. 11 (2022) 2101658. https://doi.org/https://doi.org/10.1002/adhm.202101658.

[5] J. Rädler, D. Gupta, A. Zickler, S.E.L. Andaloussi, Exploiting the biogenesis of extracellular vesicles for bioengineering and therapeutic cargo loading, Molecular Therapy 31 (2023) 1231–1250. https://doi.org/https://doi.org/10.1016/j.ymthe.2023.02.013.

[6] A. Grangier, J. Branchu, J. Volatron, M. Piffoux, F. Gazeau, C. Wilhelm, A.K.A. Silva, Technological advances towards extracellular vesicles mass production, Adv. Drug Deliv. Rev. 176 (2021) 113843.

[7] V. Syromiatnikova, A. Prokopeva, M. Gomzikova, Methods of the large-scale production of extracellular vesicles, Int. J. Mol. Sci. 23 (2022) 10522.

[8] M. Viola, M.P. Bebelman, R.G.C. Maas, W.S. de Voogt, F.J. Verweij, C.S. Seinen, S.C.A. de Jager, P. Vader, D.M. Pegtel, J. Petrus Gerardus Sluijter, Hypoxia and TNF-alpha modulate extracellular vesicle release from human induced pluripotent stem cell-derived cardiomyocytes, J. Extracell. Vesicles 13 (2024) e70000.

[9] M. Rastogi, K. Sahu, S.K. Majumder, Light assisted modulation of stem cell function and secretome production: A systematic review on current status and new avenues for regenerative medicine, Lasers Med. Sci. 40 (2025) 83.

[10] I.J.A. Evers-van Gogh, S. Alex, R. Stienstra, A.B. Brenkman, S. Kersten, E. Kalkhoven, Electric pulse stimulation of myotubes as an in vitro exercise model: Cell-mediated and non-cell-mediated effects, Sci. Rep. 5 (2015) 10944. https://doi.org/10.1038/srep10944.

[11] C. Gorgun, D. Ceresa, R. Lesage, F. Villa, D. Reverberi, C. Balbi, S. Santamaria, K. Cortese, P. Malatesta, L. Geris, Dissecting the effects of preconditioning with inflammatory cytokines and hypoxia on the angiogenic potential of mesenchymal stromal cell (MSC)-derived soluble proteins and extracellular vesicles (EVs), Biomaterials 269 (2021) 120633.

[12] C.J.K. Wong, Y.K. Tai, J.L.Y. Yap, C.H.H. Fong, L.S.W. Loo, M. Kukumberg, J. Fröhlich, S. Zhang, J.Z. Li, J.-W. Wang, A.J. Rufaihah, A. Franco-Obregón, Brief exposure to directionally-specific pulsed electromagnetic fields stimulates extracellular vesicle release and is antagonized by streptomycin: A potential regenerative medicine and food industry paradigm, Biomaterials 287 (2022) 121658. https://doi.org/https://doi.org/10.1016/j.biomaterials.2022.121658.

[13] D. Parate, A. Franco-Obregón, J. Fröhlich, C. Beyer, A.A. Abbas, T. Kamarul, J.H.P. Hui, Z. Yang, Enhancement of mesenchymal stem cell chondrogenesis with short-term low intensity pulsed electromagnetic fields, Sci. Rep. 7 (2017) 9421. https://doi.org/10.1038/s41598-017-09892-w.

[14] J.L.Y. Yap, Y.K. Tai, J. Fröhlich, C.H.H. Fong, J.N. Yin, Z.L. Foo, S. Ramanan, C. Beyer, S.J. Toh, M. Casarosa, N. Bharathy, M.P. Kala, M. Egli, R. Taneja, C.N. Lee, A. Franco-Obregón, Ambient and supplemental magnetic fields promote myogenesis via a TRPC1-mitochondrial axis: Evidence of a magnetic mitohormetic mechanism, The FASEB Journal 33 (2019) 12853–12872. https://doi.org/https://doi.org/10.1096/fj.201900057R.

[15] R.A. Louzada, J. Bouviere, L.P. Matta, J.P. Werneck-de-Castro, C. Dupuy, D.P. Carvalho, R.S. Fortunato, Redox signaling in widespread health benefits of exercise, Antioxid. Redox Signal. 33 (2020) 745–760.

[16] C. Scheele, S. Nielsen, B.K. Pedersen, ROS and myokines promote muscle adaptation to exercise, Trends in Endocrinology & Metabolism 20 (2009) 95–99.

[17] Y.K. Tai, J.N. Iversen, K.K.W. Chan, C.H.H. Fong, R.B. Abdul Razar, S. Ramanan, L.Y.J. Yap, J.N. Yin, S.J. Toh, C.J.K. Wong, P.F.A. Koh, R.Y.J. Huang, A. Franco-Obregón, Secretome from magnetically stimulated muscle exhibits anticancer potency:

Novel preconditioning methodology highlighting HTRA1 action, Cells 13 (2024). https://doi.org/10.3390/cells13050460.

[18] D. Parate, N.D. Kadir, C. Celik, E.H. Lee, J.H.P. Hui, A. Franco-Obregón, Z. Yang, Pulsed electromagnetic fields potentiate the paracrine function of mesenchymal stem cells for cartilage regeneration, Stem Cell Res. Ther. 11 (2020) 46. https://doi.org/10.1186/s13287-020-1566-5.

[19] E. Trenkenschuh, M. Richter, E. Heinrich, M. Koch, G. Fuhrmann, W. Friess, Enhancing the stabilization potential of lyophilization for extracellular vesicles, Adv. Healthc. Mater. 11 (2022) 2100538. https://doi.org/https://doi.org/10.1002/adhm.202100538.

[20] O. Rogulska, I. Vackova, S. Prazak, K. Turnovcova, S. Kubinova, L. Bacakova, P. Jendelova, Y. Petrenko, Storage conditions affect the composition of the lyophilized secretome of multipotent mesenchymal stromal cells, Sci. Rep. 14 (2024) 10243. https://doi.org/10.1038/s41598-024-60787-z.

[21] M. Laggner, A. Gugerell, C. Bachmann, H. Hofbauer, V. Vorstandlechner, M. Seibold, G. Gouya Lechner, A. Peterbauer, S. Madlener, S. Demyanets, D. Sorgenfrey, T. Ostler, M. Erb, M. Mildner, H.J. Ankersmit, Reproducibility of GMP-compliant production of therapeutic stressed peripheral blood mononuclear cell-derived secretomes, a novel class of biological medicinal products, Stem Cell Res. Ther. 11 (2020) 9. https://doi.org/10.1186/s13287-019-1524-2.

[22] Y. Zheng, C. Pan, P. Xu, K. Liu, Hydrogel-mediated extracellular vesicles for enhanced wound healing: The latest progress, and their prospects for 3D bioprinting, J. Nanobiotechnology 22 (2024) 57. https://doi.org/10.1186/s12951-024-02315-9.

[23] K. Liu, T. Veenendaal, M. Wiendels, A.M. Ruiz-Zapata, J. van Laar, R. Kyranas, H. Enting, B. van Cranenbroek, H.J.P.M. Koenen, S.M. Mihaila, E. Oosterwijk, P.H.J. Kouwer, Synthetic extracellular matrices as a toolbox to tune stem cell Secretome, ACS Appl. Mater. Interfaces 12 (2020) 56723–56730. https://doi.org/10.1021/acsami.0c16208.

[24] K. Holkar, V. Kale, G. Ingavle, Hydrogel-assisted 3D model to investigate the osteoinductive potential of MC3T3-derived extracellular vesicles, ACS Biomater. Sci. Eng. 7 (2021) 2687–2700. https://doi.org/10.1021/acsbiomaterials.1c00386.

[25] Y. Li, K.A. Kilian, Bridging the gap: From 2D cell culture to 3D microengineered extracellular matrices, Adv. Healthc. Mater. 4 (2015) 2780–2796. https://doi.org/https://doi.org/10.1002/adhm.201500427.

[26] S. Thippabhotla, C. Zhong, M. He, 3D cell culture stimulates the secretion of in vivo like extracellular vesicles, Sci. Rep. 9 (2019) 13012. https://doi.org/10.1038/s41598-019-49671-3.

[27] P. Gupta, K. Vermani, S. Garg, Hydrogels: From controlled release to pH-responsive drug delivery, Drug Discov. Today 7 (2002) 569–579. https://doi.org/https://doi.org/10.1016/S1359-6446(02)02255-9.

[28] A.Z. Nelson, B. Kundukad, W.K. Wong, S.A. Khan, P.S. Doyle, Embedded droplet printing in yield-stress fluids, Proceedings of the National Academy of Sciences 117 (2020) 5671–5679. https://doi.org/10.1073/pnas.1919363117.

[29] A.Z. Nelson, J. Xie, S.A. Khan, P.S. Doyle, Continuous embedded droplet printing in yield-stress fluids for pharmaceutical drug particle synthesis, Adv. Mater. Technol. 6 (2021) 2001245. https://doi.org/https://doi.org/10.1002/admt.202001245.

[30] P. Lefrançois, E. Ibarboure, B. Payré, E. Gontier, J.-F. Le Meins, C. Schatz, Insights into Carbopol gel formulations: Microscopy analysis of the microstructure and the influence of polyol additives, J. Appl. Polym. Sci. 132 (2015). https://doi.org/https://doi.org/10.1002/app.42761.

[31] J. Gelfi, M. Pappalardo, C. Claverys, B. Peralta, J.-L. Guérin, Safety and efficacy of an inactivated carbopol-adjuvanted goose haemorrhagic polyomavirus vaccine for domestic geese, Avian Pathology 39 (2010) 111–116. https://doi.org/10.1080/03079451003604647.

[32] M.M. Abd El-Moneam, N.A. Fathy, N.I. Ali, H.M. El Naggar, Improvements to the live-attenuated Newcastle disease virus vaccine using Carbopol® 940 as a stabilizer, Vet. World 13 (2020) 1641.

[33] A.Z. Nelson, K.S. Schweizer, B.M. Rauzan, R.G. Nuzzo, J. Vermant, R.H. Ewoldt, Designing and transforming yield-stress fluids, Curr. Opin. Solid State Mater. Sci. 23 (2019) 100758. https://doi.org/https://doi.org/10.1016/j.cossms.2019.06.002.

[34] Z. Jaworski, T. Spychaj, A. Story, G. Story, Carbomer microgels as model yield-stress fluids, 38 (2022) 881–919. https://doi.org/doi:10.1515/revce-2020-0016.

[35] T. Bhattacharjee, C.J. Gil, S.L. Marshall, J.M. Urueña, C.S. O'Bryan, M. Carstens, B. Keselowsky, G.D. Palmer, S. Ghivizzani, C.P. Gibbs, W.G. Sawyer, T.E. Angelini, Liquid-like solids support cells in 3D, ACS Biomater. Sci. Eng. 2 (2016) 1787–1795. https://doi.org/10.1021/acsbiomaterials.6b00218.

[36] D. Baruffaldi, C.F. Pirri, F. Frascella, 3D bioprinting of cell-laden carbopol bioinks, Bioprinting 22 (2021) e00135.

[37] S. Villata, F. Frascella, C.G. Gaglio, G. Nastasi, M. Petretta, C.F. Pirri, D. Baruffaldi, Self-standing gelatin-methacryloyl 3D structure using carbopol-embedded printing, Journal of Polymer Science 62 (2024) 2259–2269. https://doi.org/https://doi.org/10.1002/pol.20240037.

[38] A. Chua, W. Tan Gian Yion, E. Yeap, D. Walker, J. Hawkins, S. Khan, Rapid, automated measurement of dynamic size distributions and size-dependent growth rates of crystal ensembles within microfluidic flow cells, Cryst. Growth Des. 22 (2022). https://doi.org/10.1021/acs.cgd.1c01215.

[39] C. Chu, C. Vargas, M.C. Barbosa, S. Sommerhage, G.N. Rechberger, D. Pahovnik, E. Žagar, G.F. Schröder, S. Keller, M. Etzkorn, Capturing G protein-coupled receptors into native lipid-bilayer nanodiscs using new diisobutylene/maleic acid (DIBMA) copolymers, Methods 244 (2025) 55–64. https://doi.org/https://doi.org/10.1016/j.ymeth.2025.08.013.

[40] Y.K. Tai, C. Ng, K. Purnamawati, J.L.Y. Yap, J.N. Yin, C. Wong, B.K. Patel, P.L. Soong, P. Pelczar, J. Fröhlich, C. Beyer, C.H.H. Fong, S. Ramanan, M. Casarosa, C.P. Cerrato, Z.L. Foo, R.M. Pannir Selvan, E. Grishina, U. Degirmenci, S.J. Toh, P.J. Richards, A. Mirsaidi, K. Wuertz-Kozak, S.Y. Chong, S.J. Ferguson, A. Aguzzi, M. Monici, L. Sun, C.L. Drum, J.-W. Wang, A. Franco-Obregón, Magnetic fields modulate metabolism and gut microbiome in correlation with Pgc-1α expression: Follow-up to an in vitro magnetic mitohormetic study, The FASEB Journal 34 (2020) 11143–11167. https://doi.org/https://doi.org/10.1096/fj.201903005RR.

[41] A. Franco-Obregón, Harmonizing magnetic mitohormetic regenerative strategies: Developmental implications of a calcium–mitochondrial axis invoked by magnetic field exposure, Bioengineering 10 (2023) 1176.

[42] A.Z. Nelson, R.H. Ewoldt, Design of yield-stress fluids: A rheology-to-structure inverse problem, Soft Matter 13 (2017) 7578–7594.

[43] A.N. Beris, J.A. Tsamopoulos, R.C. Armstrong, R.A. Brown, Creeping motion of a sphere through a Bingham plastic, J. Fluid Mech. 158 (1985) 219–244.

[44] B. Géraud, L. Jørgensen, C. Ybert, H. Delanoë-Ayari, C. Barentin, Structural and cooperative length scales in polymer gels, The European Physical Journal E 40 (2017) 5. https://doi.org/10.1140/epje/i2017-11490-y.

[45] R.J. Nap, I. Szleifer, Effect of calcium ions on the interactions between surfaces end-grafted with weak polyelectrolytes, J. Chem. Phys. 149 (2018) 163309. https://doi.org/10.1063/1.5029377.

[46] M. Zhang, S. Hou, Y. Li, S. Hu, P. Yang, Swelling characterization of ionic responsive superabsorbent resin containing carboxylate sodium groups, React. Funct. Polym. 170 (2022) 105144. https://doi.org/https://doi.org/10.1016/j.reactfunctpolym.2021.105144.

[47] E. Stubblefield, G.C. Mueller, Effects of sodium chloride concentration on growth, biochemical composition, and metabolism of HeLa cells, Cancer Res. 20 (1960) 1646–1655.

[48] S. Farqarazi, M. Khorasani, The effects of synthetic and physical factors on the properties of poly(acrylic acid)-based hydrogels synthesized by precipitation polymerization technique: A review, Reviews in Chemical Engineering 40 (2024). https://doi.org/10.1515/revce-2023-0052.

[49] Y. Liu, Y. Zhu, B. Mu, Y. Wang, Z. Quan, A. Wang, Synthesis, characterization, and swelling behaviors of sodium carboxymethyl cellulose-g-poly(acrylic acid)/semi-coke superabsorbent, Polymer Bulletin 79 (2022) 935–953. https://doi.org/10.1007/s00289-021-03545-9.

[50] P. Hriberšek, K. Kogej, Effect of multivalent cations on intermolecular association of isotactic and atactic poly(methacrylic acid) chains in aqueous solutions, Polymers (Basel). 11 (2019). https://doi.org/10.3390/polym11040605.

[51] A.A. Ezhova, K. Huber, Contraction and coagulation of spherical polyelectrolyte brushes in the presence of Ag+, Mg2+, and Ca2+ cations, Macromolecules 49 (2016) 7460–7468. https://api.semanticscholar.org/CorpusID:99811012.

[52] H. Nada, Stable binding conformations of polymaleic and polyacrylic acids at a calcite surface in the presence of countercations: A metadynamics study, Langmuir 38 (2022) 7046–7057. https://doi.org/10.1021/acs.langmuir.2c00750.

[53] M.G. Vazquez de Vasquez, B.A. Wellen Rudd, M.D. Baer, E.E. Beasley, H.C. Allen, Role of hydration in magnesium versus calcium ion pairing with carboxylate: Solution and the aqueous interface, J. Phys. Chem. B 125 (2021) 11308–11319. https://doi.org/10.1021/acs.jpcb.1c06108.

[54] J.N. Iversen, Y.K. Tai, K.Y. Wu, C.J.K. Wong, H.Y. Lim, A. Franco-Obregón, Magnetically stimulated myogenesis recruits a CRY2-TRPC1 photosensitive signaling axis, Cells 14 (2025) 231.

[55] T.J. Hawke, A.P. Meeson, N. Jiang, S. Graham, K. Hutcheson, J.M. DiMaio, D.J. Garry, p21 is essential for normal myogenic progenitor cell function in regenerating skeletal muscle, American Journal of Physiology-Cell Physiology 285 (2003) C1019–C1027. https://doi.org/10.1152/ajpcell.00055.2003.

[56] I. Michailovici, H.A. Harrington, H.H. Azogui, Y. Yahalom-Ronen, A. Plotnikov, S. Ching, M.P.H. Stumpf, O.D. Klein, R. Seger, E. Tzahor, Nuclear to cytoplasmic shuttling of ERK promotes differentiation of muscle stem/progenitor cells, Development 141 (2014) 2611–2620.

[57] C.M. Brennan, A.S. Hill, M. St. Andre, X. Li, V. Madeti, S. Breitkopf, S. Garren, L. Xue, T. Gilbert, A. Hadjipanayis, DUX4 expression activates JNK and p38 MAP kinases in myoblasts, Dis. Model. Mech. 15 (2022) dmm049516.

[58] M. Louis, N. Zanou, M. Van Schoor, P. Gailly, TRPC1 regulates skeletal myoblast migration and differentiation, J. Cell Sci. 121 (2008) 3951–3959.

[59] C.-Y. Chen, H. Yin, X. Chen, T.-H. Chen, H.-M. Liu, S.-S. Rao, Y.-J. Tan, Y.-X. Qian, Y.-W. Liu, X.-K. Hu, Ångstrom-scale silver particle–embedded carbomer gel promotes wound healing by inhibiting bacterial colonization and inflammation, Sci. Adv. 6 (2020) eaba0942.

[60] S.H. Ismail, A. Hamdy, T.A. Ismail, H.H. Mahboub, W.H. Mahmoud, W.M. Daoush, Synthesis and characterization of antibacterial carbopol/ZnO hybrid nanoparticles gel, Crystals (Basel). 11 (2021) 1092.

[61] E. Karnas, M. Zając, K. Kmiotek-Wasylewska, K. Kamiński, S.-I. Yusa, S. Kędracka-Krok, P. Dudek, K. Szczubiałka, M. Nowakowska, E.K. Zuba-Surma, Polyelectrolytes are effective cryoprotectants for extracellular vesicles, ACS Appl. Mater. Interfaces 16 (2024) 70174–70186. https://doi.org/10.1021/acsami.4c11852.

[62] G. Midekessa, K. Godakumara, J. Ord, J. Viil, F. Lättekivi, K. Dissanayake, S. Kopanchuk, A. Rinken, A. Andronowska, S. Bhattacharjee, T. Rinken, A. Fazeli, Zeta potential of extracellular vesicles: Toward understanding the attributes that determine colloidal stability, ACS Omega 5 (2020) 16701–16710. https://doi.org/10.1021/acsomega.0c01582.

[63] F. Vincenzi, S. Pasquini, S. Setti, S. Salati, R. Cadossi, P.A. Borea, K. Varani, Pulsed electromagnetic fields stimulate HIF-1α-Independent VEGF release in 1321N1 human astrocytes protecting Neuron-Like SH-SY5Y cells from oxygen-glucose deprivation, Int. J. Mol. Sci. 21 (2020) 8053.

[64] J. Birch, J. Gil, Senescence and the SASP: Many therapeutic avenues, Genes Dev. 34 (2020). https://doi.org/10.1101/gad.343129.120.

[65] Y. Zhang, J. Tan, Y. Miao, Q. Zhang, The effect of extracellular vesicles on the regulation of mitochondria under hypoxia, Cell Death Dis. 12 (2021) 358.

[66] D. Su, Z. Zhao, D. Yin, Y. Ye, Promising application of pulsed electromagnetic fields on tissue repair and regeneration, Prog. Biophys. Mol. Biol. 187 (2024) 36–50.

[67] F. Tan, X. Li, Z. Wang, J. Li, K. Shahzad, J. Zheng, Clinical applications of stem cell-derived exosomes, Signal Transduct. Target. Ther. 9 (2024) 17. https://doi.org/10.1038/s41392-023-01704-0.

[68] M.S. Choudhery, T. Arif, R. Mahmood, D.T. Harris, Stem cell-based acellular therapy: insight into biogenesis, bioengineering and therapeutic applications of exosomes, Biomolecules 14 (2024). https://doi.org/10.3390/biom14070792.

[69] S.D. Dutta, T. Park, K. Ganguly, D.K. Patel, J. Bin, M.-C. Kim, K.-T. Lim, Evaluation of the sensing potential of stem cell-secreted proteins via a microchip device under electromagnetic field stimulation, ACS Appl. Bio Mater. 4 (2021) 6853–6864. https://doi.org/10.1021/acsabm.1c00561.

[70] S. Silawal, M. Gesslein, M. Willauschus, G. Schulze-Tanzil, In vitro investigation of pulsed electromagnetic field stimulation (PEMF) with MAGCELL® ARTHRO on the regulatory expression of soluble and membrane-bound complement factors and inflammatory cytokines in immortalized synovial fibroblasts, J. Pers. Med. 14 (2024). https://doi.org/10.3390/jpm14070701.

[71] D. Parate, N.D. Kadir, C. Celik, E.H. Lee, J.H.P. Hui, A. Franco-Obregón, Z. Yang, Pulsed electromagnetic fields potentiate the paracrine function of mesenchymal stem cells for cartilage regeneration, Stem Cell Res. Ther. 11 (2020) 46. https://doi.org/10.1186/s13287-020-1566-5.

[72] Y.-S. Chen, J.-J. Lee, Y.-H. Lin, Y.-J. Lin, M.-H. Yu, C.-Y. Chen, D.-Y. Cho, M.-Y. Shie, Effects of magnetic fields-stimulated 3D-Schwann cell-secreted extracellular vesicles regulate differentiation of neural stem cells and nerve regeneration, Mater. Des. 255 (2025) 114204. https://doi.org/https://doi.org/10.1016/j.matdes.2025.114204.

[73] D. Stratton, S. Lange, J.M. Inal, Pulsed extremely low-frequency magnetic fields stimulate microvesicle release from human monocytic leukaemia cells, Biochem. Biophys. Res. Commun. 430 (2013) 470–475. https://doi.org/https://doi.org/10.1016/j.bbrc.2012.12.012.

[74] P. Shi, H. Gao, Z. Cheng, K. Zhao, Y. Chen, X. Chen, W. Gan, A. Zhang, C. Yang, Y. Zhang, Static magnetic field-modulated mesenchymal stem cell-derived mitochondria-containing microvesicles for enhanced intervertebral disc degeneration therapy, J. Nanobiotechnology 22 (2024) 457.

[75] Y. Xu, Q. Wang, X.-X. Wang, X.-N. Xiang, J.-L. Peng, C.-Q. He, H.-C. He, The effect of different frequencies of pulsed electromagnetic fields on cartilage repair of adipose mesenchymal stem cell–derived exosomes in osteoarthritis, Cartilage 13 (2022) 200–212. https://doi.org/10.1177/19476035221137726.

[76] M. Trentini, U. D'amora, A. Ronca, L. Lovatti, J.L. Calvo-Guirado, D. Licastro, S.D. Monego, L.G. Delogu, M.R. Wieckowski, S. Barak, Bone regeneration revolution: Pulsed electromagnetic field modulates macrophage-derived exosomes to attenuate osteoclastogenesis, Int. J. Nanomedicine (2024) 8695–8707.

Supplementary Files

This is a list of supplementary files associated with this preprint. Click to download.

- SupplementaryFileBlots.pdf
- SupportingInformationnpj2026uploadready.docx